An Inverse Dynamics Optimization Formulation With Recursive B-Spline Derivatives and Partition of Unity Contacts: Demonstration Using Two-Dimensional Musculoskeletal Arm and Gait

Yujiang Xiang[1]
School of Mechanical and Aerospace Engineering,
Oklahoma State University,
Stillwater, OK 74078
e-mail: yujiang.xiang@okstate.edu

In this study, an inverse dynamics optimization formulation and solution procedure is developed for musculoskeletal simulations. The proposed method has three main features: high order recursive B-spline interpolation, partition of unity, and inverse dynamics formulation. First, joint angle and muscle force profiles are represented by recursive B-splines. The formula for high order recursive B-spline derivatives is derived for state variables calculation. Second, partition of unity is used to handle the multicontact indeterminacy between human and environment during the motion. The global forces and moments are distributed to each contacting point through the corresponding partition ratio. Third, joint torques are inversely calculated from equations of motion (EOM) based on state variables and contacts to avoid numerical integration of EOM. Therefore, the design variables for the optimization problem are joint angle control points, muscle force control points, knot vector, and partition ratios for contacting points. The sum of muscle stress/activity squared is minimized as the cost function. The constraints are imposed for human physical constraints and task-based constraints. The proposed formulation is demonstrated by simulating a trajectory planning problem of a planar musculoskeletal arm with six muscles. In addition, the gait motion of a two-dimensional musculoskeletal model with sixteen muscles is also optimized by using the approach developed in this paper. The gait optimal solution is obtained in about 1 min central processing unit (CPU) time. The predicted kinematics, kinetics, and muscle forces have general trends that are similar to those reported in the literature. [DOI: 10.1115/1.4042436]

Keywords: inverse dynamics optimization, high order B-spline, B-spline derivative, partition of unity, musculoskeletal arm, musculoskeletal gait

1 Introduction

Dynamic optimization of a musculoskeletal model is a challenging problem. The difficulties are threefold: First, the appropriate cost function and constraints; second, the correct muscle-tendon property; and third, the optimization formulation and solution procedure. The last difficulty affects the computation efficiency most, and the key component is how to treat equations of motion (EOM) in the optimization process. Recently, there has been significant progress on reducing the computational effort for musculoskeletal motion prediction, thanks to various optimization formulations and large-scale optimization algorithms development [1–11].

Pure forward dynamics optimization usually requires heavy computational effort [12]. The following four formulations can effectively reduce the computational cost and have become popular recently: direct collocation method [1,2,7], inverse dynamics optimization [4–6,10,13], mixed forward and inverse dynamics optimization [8,9], and mixed forward dynamics simulation and feedback control [14,15]. It is important to note that both accuracy and efficiency are important for musculoskeletal motion prediction. Tracking joint angles and ground reaction forces (GRFs) in the optimization process can predict more accurate muscle activities. It also facilitates a practical implementation [5,7,15–17]. However, definitely, it sacrifices some power of prediction since tracking term is included in the cost function. In contrast, a purely optimization-based prediction model can show more cause-and-effect. But the human central nervous system is complicated, it is hard for such a model to be completely accurate compared with experimental results. Thus, researchers need to balance the two sides of tracking and prediction based on applications.

In this study, an inverse dynamics optimization formulation is developed for musculoskeletal models. Partition of unity is used to handle the multicontact indeterminacy between human and environment. A high order recursive B-spline interpolation with derivatives is developed for state variable calculation and sensitivity analysis. The recursive interpolation is efficient and easy-to-implement to discretize joint angle and muscle force profiles. Most importantly, the higher order smoothness makes the EOM and symmetry/continuity equality constraints much easier to satisfy for the optimization [6]. Design sensitivities are implemented analytically for the gradient-based optimization algorithm [11]. The developed formulation can treat open-loop and closed-loop mechanical systems with multiple contacts using partition of unity. The proposed formulation is used to solve two optimal trajectory planning problems for planar musculoskeletal arm and gait models. Muscle stress/activity squared is minimized subject to the physical and task-based limits. The two-dimensional (2D) gait optimal solution is obtained in about 1 min central processing unit (CPU) time. The optimal solutions are partially verified with the solutions available in the literature.

2 Musculoskeletal Dynamics

2.1 Equations of Motion. The musculoskeletal model has n joints and m muscle-tendons among which n_b is the number of global translation and rotation joints in inertial frame. The Lagrange equation for the musculoskeletal model can be written in vector-matrix form [6,18]

$$\boldsymbol{\tau}_{SK} = \boldsymbol{M}(\boldsymbol{q})\ddot{\boldsymbol{q}} + \boldsymbol{V}(\boldsymbol{q},\dot{\boldsymbol{q}}) + \boldsymbol{G}(\boldsymbol{q}) + \sum_i \boldsymbol{J}_{Ci}^{\mathrm{T}}\left[\boldsymbol{F}_{Ci}^{\mathrm{T}}, \boldsymbol{M}_{Ci}^{\mathrm{T}}\right]^{\mathrm{T}} + \sum_j \boldsymbol{J}_{Aj}^{\mathrm{T}}\left[\boldsymbol{F}_{Aj}^{\mathrm{T}}, \boldsymbol{M}_{Aj}^{\mathrm{T}}\right]^{\mathrm{T}} \tag{1a}$$

$$\boldsymbol{\tau}_{MT} = \boldsymbol{R}(\boldsymbol{q})\boldsymbol{f} \tag{1b}$$

$$\boldsymbol{\tau}_{SK} + \boldsymbol{\tau}_{MT} = \boldsymbol{0} \tag{1c}$$

where $\boldsymbol{\tau}_{SK}$ is the skeleton joint torque $(n \times 1)$; $\boldsymbol{M}(\boldsymbol{q})$ is the system mass matrix $(n \times n)$; $\boldsymbol{V}(\boldsymbol{q},\dot{\boldsymbol{q}})$ is the centrifugal and Coriolis loading $(n \times 1)$; $\boldsymbol{G}(\boldsymbol{q})$ is the gravitational loading $(n \times 1)$; $\boldsymbol{J}_{Ci}$ is the augmented Jacobian matrix $(6 \times n)$ for the ith contact point where contact force $\boldsymbol{F}_{Ci}$ and moment $\boldsymbol{M}_{Ci}$ applied; similarly, $\boldsymbol{J}_{Aj}$ is the augmented Jacobian matrix $(6 \times n)$ for the jth given applied external force $\boldsymbol{F}_{Aj}$ and moment $\boldsymbol{M}_{Aj}$; $\boldsymbol{\tau}_{MT}$ is the muscular joint torque $(n \times 1)$; $\boldsymbol{f}$ is the muscle-tendon force $(m \times 1)$; and $\boldsymbol{R}(\boldsymbol{q})$ is the matrix of muscular moment arms $(n \times m)$. $(\cdots)^{\mathrm{T}}$ denotes the transpose operation.

2.2 Contact Model: Partition of Unity. Contact force and moment are inversely calculated from unbalanced global skeletal joint torque $\boldsymbol{\tau}_{SK}^{B}$, $(n_b \times 1)$, through the following procedures [10,19]:

Step 1. Given the joint state variables $(\boldsymbol{q},\dot{\boldsymbol{q}},\ddot{\boldsymbol{q}})$ and external applied force and moment $(\boldsymbol{F}_A,\boldsymbol{M}_A)$, excluding contact force and

[1]Corresponding author.

Manuscript received September 2, 2018; final manuscript received December 19, 2018; published online January 31, 2019. Assoc. Editor: Guy M. Genin.

moment $(\boldsymbol{F}_C, \boldsymbol{M}_C)$, the skeletal joint torque $\boldsymbol{\tau}^0_{SK}$, $(n \times 1)$, can be calculated as

$$\boldsymbol{\tau}^0_{SK} = \boldsymbol{M}(\boldsymbol{q})\ddot{\boldsymbol{q}} + \boldsymbol{V}(\boldsymbol{q}, \dot{\boldsymbol{q}}) + \boldsymbol{G}(\boldsymbol{q}) + \sum_j \boldsymbol{J}^{\mathrm{T}}_{Aj}\left[\boldsymbol{F}^{\mathrm{T}}_{Aj}, \boldsymbol{M}^{\mathrm{T}}_{Aj}\right]^{\mathrm{T}} \tag{2}$$

Step 2. For $\boldsymbol{\tau}^0_{SK}$, the corresponding global force and moment vector is $\boldsymbol{\tau}^B_{SK} = \left[\boldsymbol{F}^{\mathrm{T}}_B, \boldsymbol{M}^{\mathrm{T}}_B\right]^{\mathrm{T}}$, where $\boldsymbol{F}_B$ is the global translational joint torque and $\boldsymbol{M}_B$ is the global rotational joint torque. $\boldsymbol{\tau}^B_{SK}$ is usually not zero and needs to be balanced (become zero) by contact forces.

Step 3. For each contact point, there is a corresponding decomposed global force and moment term $\rho_i \boldsymbol{\tau}^B_{SK}$, where ρ_i is the partition ratio for the ith contact, and

$$\sum \rho_i = 1 \tag{3}$$

Step 4. Each decomposed global force and moment $\rho_i \boldsymbol{\tau}^B_{SK}$ is transferred to corresponding contact point location $\boldsymbol{r}_{Ci}(\boldsymbol{q})$, which is a vector from contact point to global force location, to obtain contact force and moment as

$$\begin{bmatrix} \boldsymbol{F}_{Ci} \\ \boldsymbol{M}_{Ci} \end{bmatrix} = \begin{bmatrix} -\rho_i \boldsymbol{F}_{Bi} \\ -\rho_i \boldsymbol{M}_{Bi} - \boldsymbol{r}_{Ci}(\boldsymbol{q}) \times \rho_i \boldsymbol{F}_{Bi} \end{bmatrix} \tag{4}$$

3 Recursive B-Spline Discretization

A joint profile $q(t)$ is parameterized by using B-spline curve as follows:

$$q(t) = \sum_{i=1}^{s} N^p_i(t) P_i \tag{5}$$

where $N^p_i(t)$ is the p degree basis function associated with the ith control point P_i and s is the number of control points.

3.1 Recursive B-Spline Basis Function. The basis function is constructed from the knot vector $\boldsymbol{t} = \{t_1, t_2, \ldots, t_{s+p+1}\}$. The p degree basis function is calculated recursively starting from the zero-degree basis function $N^0_i(t)$ as [20]

$$N^0_i(t) = \begin{cases} 1 & \text{for} \quad t \in [t_i, t_{i+1}) \\ 0 & \text{otherwise} \end{cases} \tag{6a}$$

$$N^p_i(t) = \frac{t - t_i}{t_{i+p} - t_i} N^{p-1}_i(t) + \frac{t_{i+p+1} - t}{t_{i+p+1} - t_{i+1}} N^{p-1}_{i+1}(t) \tag{6b}$$

3.2 Recursive B-Spline Time Derivatives. The first time derivative of B-spline curve defined in Eq. (5) can be evaluated as

$$\dot{q}(t) = \sum_{i=1}^{m} N^p_i(t)' P_i \tag{7}$$

where the first time derivative of the basis function can be computed as [21]

$$N^p_i(t)' = \frac{p}{t_{i+p} - t_i} N^{p-1}_i(t) - \frac{p}{t_{i+p+1} - t_{i+1}} N^{p-1}_{i+1}(t) \tag{8}$$

Higher time derivative of the curve is calculated through the higher derivative of the basis function which is constructed recursively as

$$\frac{d^{(k)}}{dt^{(k)}} q(t) = \sum_{i=1}^{m} N^{p,k}_i(t) P_i \tag{9a}$$

$$N^{p,1}_i(t) = \frac{p}{t_{i+p} - t_i} N^{p-1}_i(t) - \frac{p}{t_{i+p+1} - t_{i+1}} N^{p-1}_{i+1}(t) \tag{9b}$$

$$N^{p,k}_i(t) = \frac{p}{t_{i+p} - t_i} N^{p-1,k-1}_i(t) - \frac{p}{t_{i+p+1} - t_{i+1}} N^{p-1,k-1}_{i+1}(t) \tag{9c}$$

where the superscript k denotes the kth time derivative and $k \geq 2$.

4 Inverse Dynamics Optimization

For musculoskeletal motion prediction, the design variables $\boldsymbol{x}$ are joint angle control points $\boldsymbol{P}_q$, muscle-tendon force control points $\boldsymbol{P}_f$, global force and moment partition ratios $\boldsymbol{\rho}$, and B-spline knot vector $\boldsymbol{t}$, where $\boldsymbol{x} = \begin{bmatrix} \boldsymbol{P}^{\mathrm{T}}_q & \boldsymbol{P}^{\mathrm{T}}_f & \boldsymbol{\rho}^{\mathrm{T}} & \boldsymbol{t}^{\mathrm{T}} \end{bmatrix}^{\mathrm{T}}$.

The cost function E_1 for human performance measure is the integral of the muscle-tendon stress squared as in Eq. (10), where PCSA_i is the physiological cross-sectional area of the ith muscle [22]. The cost function E_2 is the integral of the normalized muscle-tendon force squared as in Eq. (11). The normalized muscle-tendon force is usually referred to as the muscle activity [4,23], where $f^{\max}_i$ is the ith muscle-tendon strength obtained from the literature [24]

$$E_1 = \sum_i \int_0^T \left(\frac{f_i(t)}{\mathrm{PCSA}_i}\right)^2 dt \tag{10}$$

$$E_2 = \sum_i \int_0^T \left(\frac{f_i(t)}{f^{\max}_i}\right)^2 dt \tag{11}$$

The physics-based constraints for musculoskeletal motion include joint angle limit, joint torque limit, muscle-tendon force limit, musculoskeletal EOM, bounds on design variables, and partition of unity as shown in the following equations:

$$\boldsymbol{q}^L \leq \boldsymbol{q} \leq \boldsymbol{q}^U \tag{12}$$

$$\boldsymbol{\tau}^L_{SK} \leq \boldsymbol{\tau}_{SK} \leq \boldsymbol{\tau}^U_{SK} \tag{13}$$

$$0 \leq \boldsymbol{f} \leq \boldsymbol{f}^{\max} \tag{14}$$

$$\boldsymbol{\tau}_{SK} + \boldsymbol{\tau}_{MT} = \boldsymbol{0} \tag{15}$$

$$\boldsymbol{x}^L \leq \boldsymbol{x} \leq \boldsymbol{x}^U \tag{16}$$

$$\sum \rho_i = 1 \tag{17}$$

where $\boldsymbol{q}^L$ and $\boldsymbol{q}^U$ are joint angle lower and upper limits, respectively; and $\boldsymbol{\tau}^L_{SK}$ and $\boldsymbol{\tau}^U_{SK}$ are skeletal joint torque lower and upper limits, respectively.

5 Numerical Examples

In this study, the skeleton is constructed using Denavit–Hartenberg method [25]. The kinematics is computed recursively and the EOM (Eq. (1)) is implemented with recursive Lagrange equations [26]. The sequential quadratic programming (SQP) algorithm in SNOPT is used to solve the optimization problem [11]. Analytical gradients are provided for all cost function and constraints for use in the optimization process. The optimality and feasibility tolerances are set to $\varepsilon = 10^{-3}$ in SNOPT. The constant starting points for design variables $\boldsymbol{x}$ are used in the optimization: $P_{qi} = 0$, $P_{fi} = 10$, $\rho_i = 0.5$, and $\boldsymbol{t}$ is evenly distributed between 0 and 1.

5.1 Musculoskeletal Planar Arm Motion Prediction. The musculoskeletal planar arm model [27] consists of two body segments (upper arm and forearm) and the relative joint angles $\boldsymbol{q}$ (shoulder q_1 and elbow q_2) are selected as skeleton degrees-of-freedom (DOF) as shown in Fig. 1(*a*). Six muscle groups are included in the model: *anterior deltoid (AD)*, *posterior deltoid (PD)*, *brachialis (Brach)*, *lateral triceps (LT)*, *long head of biceps (LHB)*, and *long head of triceps (LHT)*. The arm skeleton physical parameters are obtained from Refs. [27] and [28], and the muscle properties are obtained from Ref. [22]. The additional joint frictional torques in Ref. [27], which are proportional to joint angular velocities, are also added into the right-hand side of

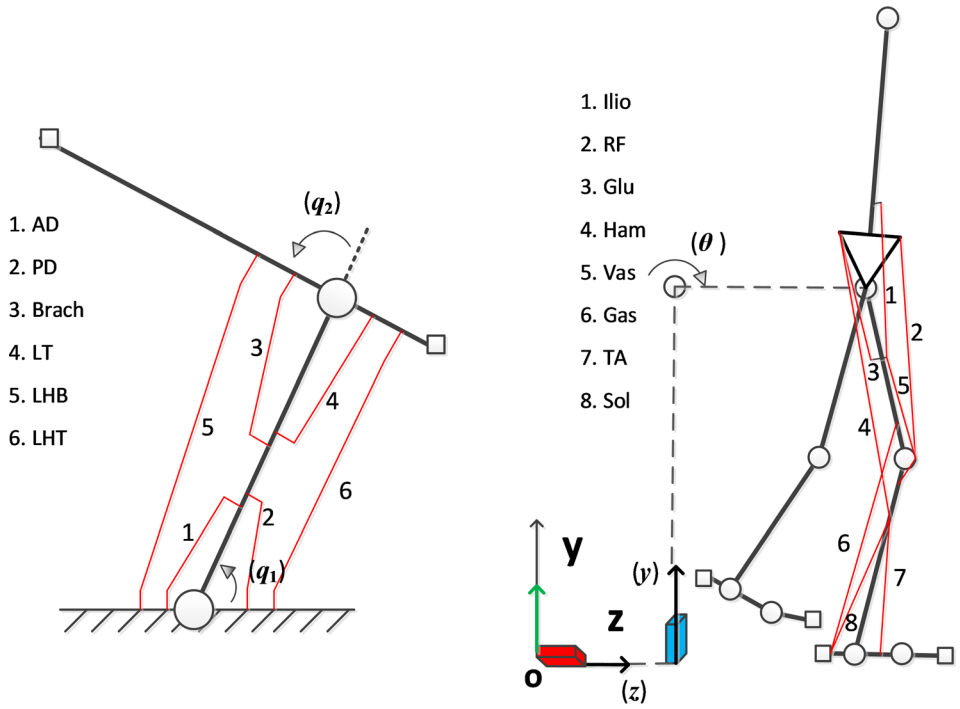

Fig. 1 Two-dimensional musculoskeletal arm (*a*) and gait (*b*) models

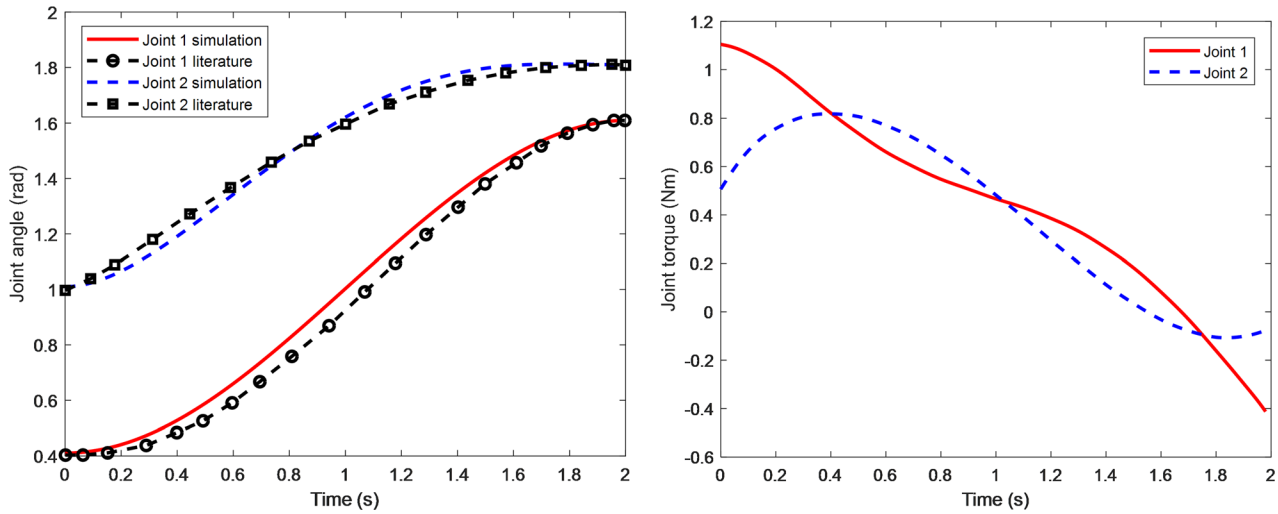

Fig. 2 Arm joint angle and torque profiles

Eq. (1*a*). The arm is assumed to lie in the horizontal plane moving from the initial position $\begin{bmatrix} q_1(0) & q_2(0) \end{bmatrix}$ to the final position $\begin{bmatrix} q_1(T) & q_2(T) \end{bmatrix}$ in the time interval T. In addition, the arm is at rest at the initial and final points. The additional task-based constraints for the arm motion are defined as

$$\begin{bmatrix} \boldsymbol{q}^{\mathrm{T}}(0) & \dot{\boldsymbol{q}}^{\mathrm{T}}(0) \end{bmatrix} = \begin{bmatrix} 0.4 & 1.0\ 0 & 0 \end{bmatrix} \tag{18}$$

$$\begin{bmatrix} \boldsymbol{q}^{\mathrm{T}}(T) & \dot{\boldsymbol{q}}^{\mathrm{T}}(T) \end{bmatrix} = \begin{bmatrix} 1.6 & 1.8\ 0 & 0 \end{bmatrix} \tag{19}$$

In this example, the EOM (Eq. (1)) is simplified because there are no global DOF, gravity (horizontal planar motion), and external contact force and moment. Cubic B-splines (degree $p = 3$) are used for both joint angle and muscle-tendon force profiles time discretization with the same knot vector. Each joint angle and muscle-tendon force is represented by 13 control points and 17 kn with the multiplicity (4 repeated knots at initial and final time points, respectively). In addition, there are four additional time nodes between any two adjacent distinguished knots, and this results in a total of 51 temporal nodes to evaluate the cost function and constraints values in the time interval T. Given the total time $T = 2$ s, the knots are assumed evenly distributed except the repeated knots at the boundaries.

The musculoskeletal arm motion prediction problem is formulated as to find the optimal design variables $\boldsymbol{x} = \begin{bmatrix} \boldsymbol{P}_q^{\mathrm{T}} & \boldsymbol{P}_f^{\mathrm{T}} \end{bmatrix}^{\mathrm{T}}$, and to minimize the cost function Eq. (10) subject to physics-based constraints Eqs. (12)–(16) and task-based constraints Eqs. (18) and (19). There are in total 105 design variables and 194 nonlinear constraints. The optimal solution is obtained in 0.68 CPU seconds on a 3.90 GHz Dell Inspiron desktop computer (Intel Core i3-7100 processor).

The optimal joint angle and torque profiles are shown in Fig. 2. The arm muscle forces are depicted in Fig. 3. The arm's trajectory

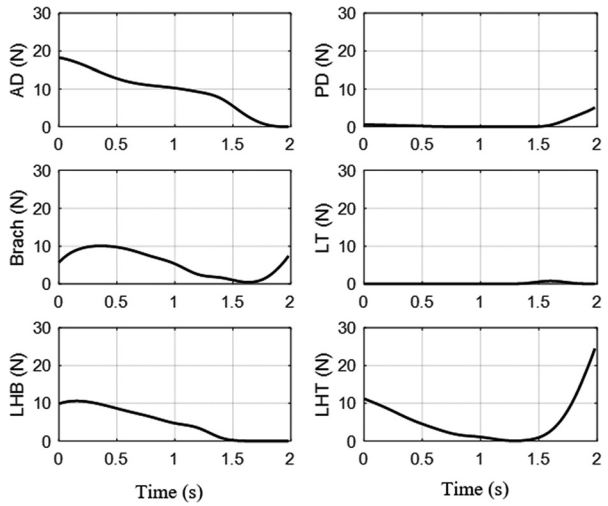

Fig. 3 Arm muscle-tendon forces

is illustrated in Fig. 4(*a*). To verify the EOM equality constraint (Eq. (15)), its value is plotted every 0.01 s at the optimal solution in Fig. 4(*b*).

5.2 Musculoskeletal Gait Prediction. The musculoskeletal gait model [8,29] consists of nine body segments (trunk, thighs, shanks, hind feet, and forefeet) and has twelve kinematic DOF (three global joints, z, y, θ, and nine physical joints) as shown in Fig. 1(*b*). Eight muscle groups are included in each leg: *iliopsoas (Ilio)*, *glutei (Glu)*, *hamstrings (Ham)*, *rectus femoris (RF)*, *vasti (Vas)*, *gastrocnemius (Gas)*, *soleus (Sol)*, and *tibialis anterior (TA)*. The anthropometric data for a 50th percentile male obtained from GEBOD™ are used in this study [10], and the muscle properties are obtained from Ref. [24]. The model is assumed to move in the sagittal plane where the gait is bilateral symmetric so that only half a gait cycle is simulated. The gait task-based constraints include bilateral symmetry constraint, feet contact position constraint, feet penetration constraint, zero-moment-point (ZMP) balance constraint, and vertical spine constraint [8] as illustrated in the following equations:

$$\begin{bmatrix} \boldsymbol{q}^{\mathrm{T}}(0) & \dot{\boldsymbol{q}}^{\mathrm{T}}(0) & \ddot{\boldsymbol{q}}^{\mathrm{T}}(0) & \boldsymbol{f}^{\mathrm{T}}(0) & \boldsymbol{\rho}^{\mathrm{T}}(0) \end{bmatrix} = \begin{bmatrix} \boldsymbol{q}_S^{\mathrm{T}}(T) & \dot{\boldsymbol{q}}_S^{\mathrm{T}}(T) & \ddot{\boldsymbol{q}}_S^{\mathrm{T}}(T) & \boldsymbol{f}_S^{\mathrm{T}}(T) & \boldsymbol{\rho}_S^{\mathrm{T}}(T) \end{bmatrix} \tag{20}$$

$$\boldsymbol{p}_C(\boldsymbol{q}, t) = \boldsymbol{p}_S(t) \tag{21}$$

$$\boldsymbol{p}_H(\boldsymbol{q}, t) \geq \boldsymbol{0} \tag{22}$$

$$\boldsymbol{p}_{\mathrm{ZMP}}(\boldsymbol{q}, \dot{\boldsymbol{q}}, \ddot{\boldsymbol{q}}, t) \in \mathrm{FSR}(t) \tag{23}$$

$$q_{\mathrm{spine}}(t) \in [0\,\mathrm{deg}\ 5\,\mathrm{deg}] \tag{24}$$

where $\boldsymbol{q}_S$ is the corresponding symmetric joints for $\boldsymbol{q}$ vector; $\boldsymbol{f}_S$ is the symmetric muscle-tendon force; $\boldsymbol{\rho}_S$ is the symmetric partition ratio; $\boldsymbol{p}_C$ is the foot point position; $\boldsymbol{p}_S$ is the specified foot contact position which depends on the given step length (0.54 m in this case); $\boldsymbol{p}_H$ is the foot point height; $\boldsymbol{p}_{\mathrm{ZMP}}$ is ZMP position; and FSR denotes foot support region.

Hexic B-splines (degree $p = 6$) are used for joint angle and muscle-tendon force time discretization with nine control points and 16 kn. In addition, there are three additional time nodes between any two adjacent distinguished knots, and this results in a total of ten temporal nodes in the time interval T. The total time duration T is divided into three physical segments: double support duration αT, hind foot single support duration $\beta(1-\alpha)T$, and forefoot single support duration $(1-\beta)(1-\alpha)T$. Thus, the knot vector is a function of $\boldsymbol{t} = \boldsymbol{t}(\alpha, \beta, T)$.

The musculoskeletal gait prediction problem is formulated as to find the optimal design variables $\boldsymbol{x} = \begin{bmatrix} \boldsymbol{P}_q^{\mathrm{T}} & \boldsymbol{P}_f^{\mathrm{T}} & \boldsymbol{\rho}^{\mathrm{T}} & \alpha & \beta & T \end{bmatrix}^{\mathrm{T}}$, and to minimize the cost function Eq. (11) subject to physics-based constraints Eqs. (12)–(17) and task-based constraints Eqs. (20)–(24). There are in total 259 design variables and 515 nonlinear constraints. The optimal solutions are obtained in 42.72 CPU seconds.

The optimal joint angle, torque, and GRF profiles are shown in Fig. 5. The leg muscle activities are depicted in Fig. 6. The gait motion trajectory is illustrated in Fig. 7.

6 Conclusion and Discussion

In this paper, an inverse dynamics optimization formulation is presented, and the proposed method is successfully applied to planar musculoskeletal arm and gait simulations. The gait optimal solution is obtained in about 1 min CPU time. Partition of unity is

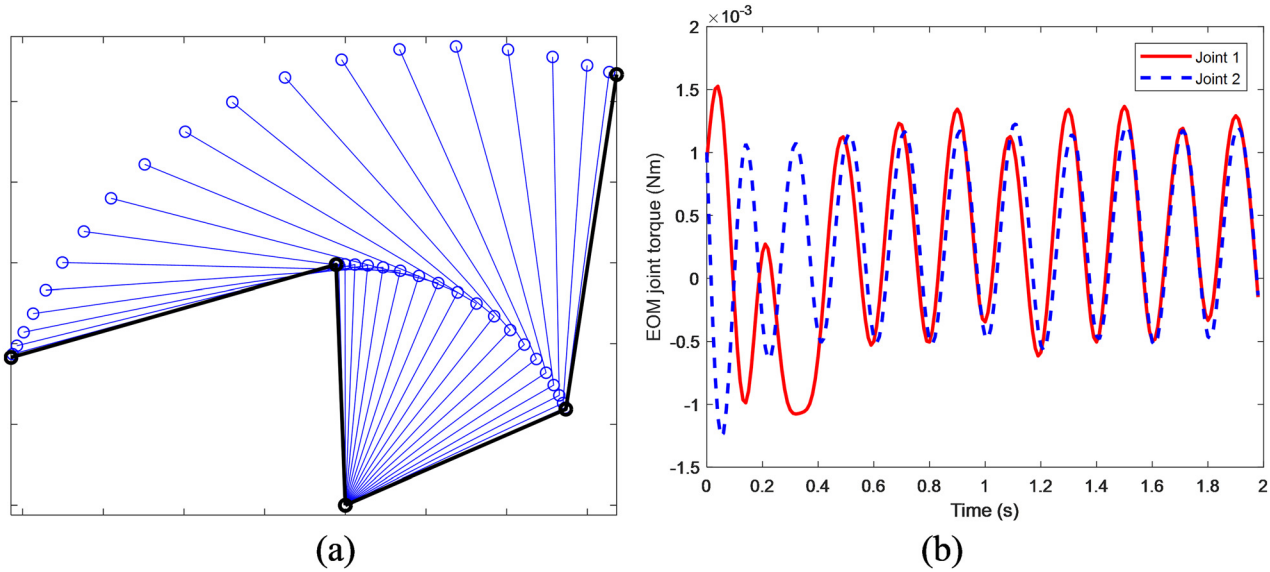

Fig. 4 Arm motion trajectory (*a*) and EOM constraint (*b*)

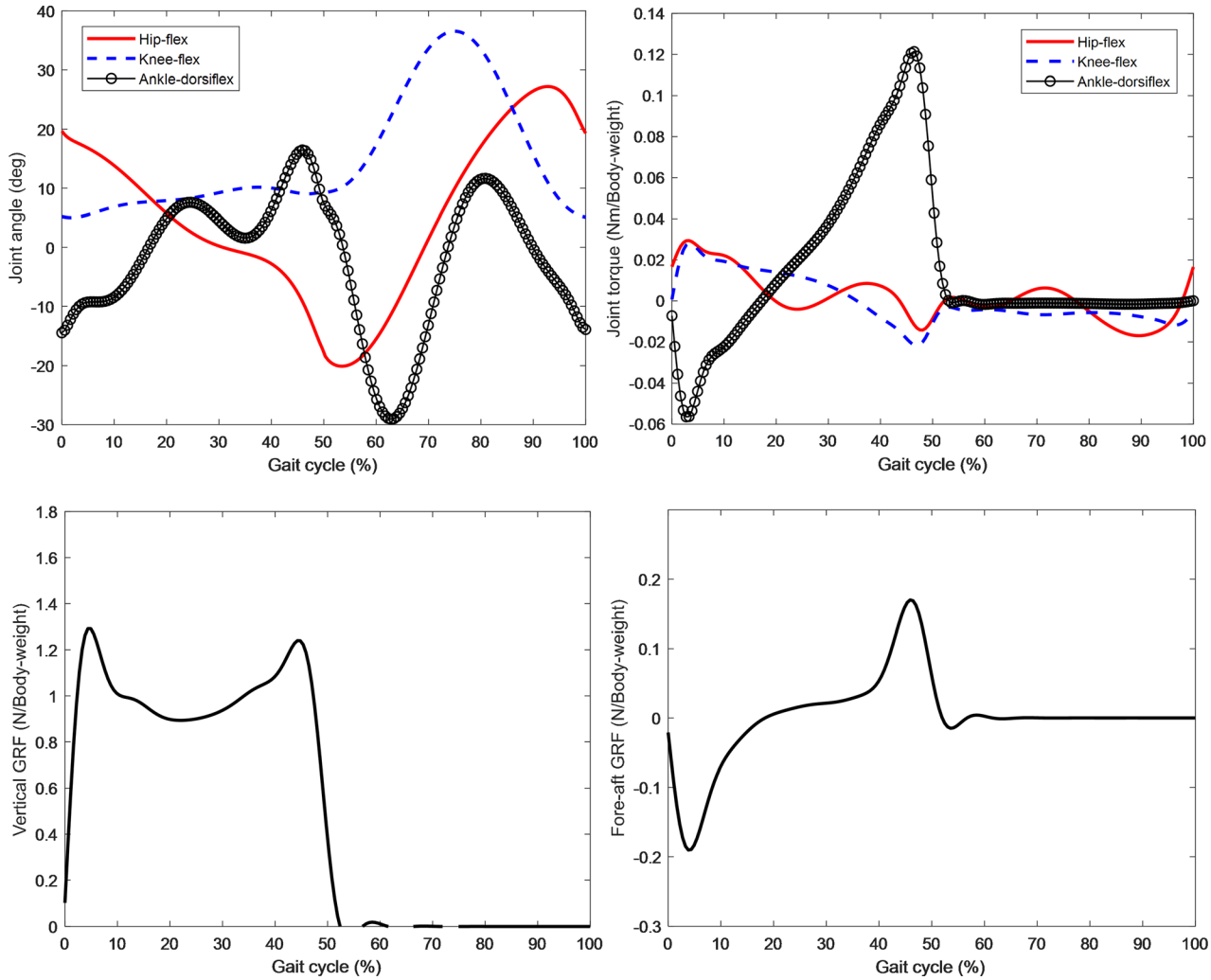

Fig. 5 Gait joint angle, torque, and GRF profiles

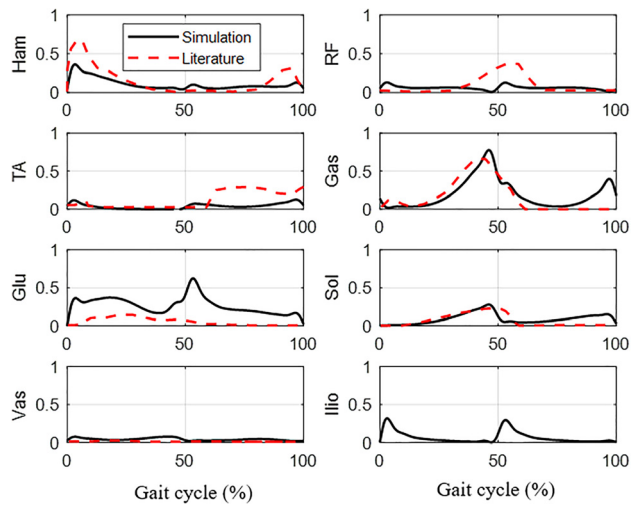

Fig. 6 Gait muscle-tendon activities ($f_i(t)/f_i^{max}$ [23])

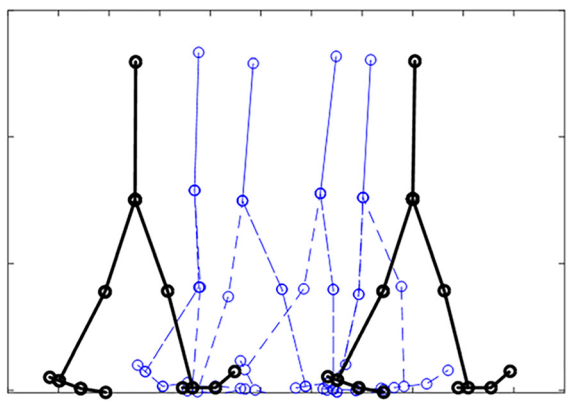

Fig. 7 Gait motion trajectory

used to solve the indeterminacy of double support phase of gait. This method is general and can be extended to multicontact situations between human and environment. New higher order recursive B-spline derivatives are derived. This is quite important for making the symmetry and EOM equality constraints satisfied due to extra smoothness of the interpolated curve, which can be seen from EOM constraint value in Fig. 4(*b*) and symmetry constraints in Figs. 5 and 6 (initial and final values of the curves). In addition, the recursive formulation makes the B-spline implementation easier.

Inverse dynamics optimization formulation can effectively reduce the number of equality constraints compared to direct collocation method. For the partition of unity constraint in Eq. (17), since the partition ratios are design variables, Eq. (17) is

implemented in the way that the last ratio is equal to 1 minus the sum of all other ratios, so that this equality constraint is eliminated in the implementation [19]. Therefore, for physical constraints, the only unavoidable equality constraint is EOM in Eq. (15). Higher order B-spline interpolation can reduce the chance of infeasible solutions for this equality constraint.

For musculoskeletal arm motion planning, the predicted joint angles match well with the solution in the literature [27,28]. However, there are some discrepancies for the joint torques between the simulation and the data in the literature, likewise for the muscle forces [27]. This may be due to different solution methods for the optimization. Sharifi et al. [27] used indirect optimal control approach: variation of extremals. In contrast, inverse dynamics optimization method is used in this study. Suzuki et al. [28] did not report joint torque and muscle-tendon forces. In Fig. 4(*b*), we can see that EOM between the muscle-tendon torque and the skeleton torque are satisfied very well within 10^{-3} N magnitude of error.

For musculoskeletal gait simulation, the predicted joint angle, torque, and GRF have trends similar to the literature [10,30] except the second peak value of knee joint angle during swing phase. In Xiang et al. [10], there was discussion on specifying a midswing angle constraint to increase the second peak value of knee joint to avoid foot drag and its effect on gait kinematics and kinetics. A reasonable gait motion is generated as shown in Fig. 7. In addition, Fig. 6 shows muscle activities compared to the data available in the literature [23]. The glutei muscle shows higher activity during gait cycle compared to the value in the literature. This may be due to the inaccuracy of the 2D model and the small knee flexion angle during the swing phase.

It is noted that there are some limitations in this study: first, only 2D models are used to demonstrate the method; second, muscle activation and contraction dynamics are not modeled; third, some discrepancies are observed between the prediction and the experimental data available in the literature. Although studies [6,8] show that contraction dynamics can be modeled using inverse formulation based on state variables and muscle-tendon forces, the gradients of such problem are discontinuous due to the inherent piecewise physiological muscle property [6,8,31]. This might cause some difficulties for gradient-based optimization [11,32]. Instead, approximate continuous muscle-tendon property might be used in this case [32,33] or nongradient based optimization methods could be employed [34]. For future research, (1) tracking term in cost function will be explored; (2) 3D musculoskeletal model with wrapping will be developed; (3) multicontact task will be validated; (4) muscle activation and contraction dynamics will be included; and (5) the proposed methodology might be able to open some opportunities for predictive musculoskeletal research and application.

Funding Data

- Directorate for Engineering NSF (Grant Nos. 1700865, 1849279, and 1703093, Funder ID. 10.13039/100000084).

References

[1] De Groote, F., Kinney, A. L., Rao, A. V., and Fregly, B. J., 2016, "Evaluation of Direct Collocation Optimal Control Problem Formulations for Solving the Muscle Redundancy Problem," Ann. Biomed. Eng., **44**(10), pp. 2922–2936.

[2] Ackermann, M., and van den Bogert, A. J., 2010, "Optimality Principles for Model-Based Prediction of Human Gait," J. Mech., **43**(6), pp. 1055–1060.

[3] Bessonnet, G., Marot, J., Seguin, P., and Sardain, P., 2010, "Parametric-Based Dynamic Synthesis of 3D-Gait," Robotica, **28**(4), pp. 563–581.

[4] Farahani, S. D., Andersen, M. S., de Zee, M., and Rasmussen, J., 2016, "Optimization-Based Dynamic Prediction of Kinematic and Kinetic Patterns for a Human Vertical Jump From a Squatting Position," Multibody Syst. Dyn., **36**(1), pp. 37–65.

[5] Fregly, B. J., Reinbolt, J. A., Rooney, K. L., Mitchell, K. H., and Chmielewski, T. L., 2007, "Design of Patient-Specific Gait Modifications for Knee Osteoarthritis Rehabilitation," IEEE Trans. Biomed. Eng., **54**(9), pp. 1687–1695.

[6] Garcia-Vallejo, D., and Schiehlen, W., 2012, "3D-Simulation of Human Walking by Parameter Optimization," Arch. Appl. Mech., **82**, pp. 533–556.

[7] Lin, Y. C., and Pandy, M. G., 2017, "Three-Dimensional Data-Tracking Dynamic Optimization Simulations of Human Locomotion Generated by Direct Collocation," J. Mech., **59**, pp. 1–8.

[8] Shourijeh, M. S., and McPhee, J., 2014, "Forward Dynamic Optimization of Human Gait Simulations: A Global Parameterization Approach," ASME J. Comput. Nonlinear Dyn., **9**(3), p. 031018.

[9] Shourijeh, M. S., Smale, K. B., Potvin, B. M., and Benoit, D. L., 2016, "A Forward-Muscular Inverse-Skeletal Dynamics Framework for Human Musculoskeletal Simulations," J. Mech., **49**, pp. 1718–1723.

[10] Xiang, J., Arora, J. S., and Abdel-Malek, K., 2011, "Optimization-Based Prediction of Asymmetric Human Gait," J. Mech., **44**(4), pp. 683–693.

[11] Gill, P. E., Murray, W., and Saunders, M. A., 2005, "SNOPT: An SQP Algorithm for Large-Scale Constrained Optimization," SIAM J. Optim., **47**(1), pp. 99–131.

[12] Pandy, M. G., 2001, "Computer Modeling and Simulation of Human Movement," Annu. Rev. Biomed. Eng., **3**(1), pp. 245–273.

[13] Xiang, Y., Arora, J. S., Rahmatalla, S., and Abdel-Malek, K., 2009, "Optimization-Based Dynamic Human Walking Prediction: One Step Formulation," Int. J. Numer. Methods Eng., **79**(6), pp. 667–695.

[14] Thelen, D. G., Anderson, F. C., and Delp, S. L., 2003, "Generating Dynamic Simulations of Movement Using Computed Muscle Control," J. Mech., **36**(3), pp. 321–328.

[15] Thelen, D. G., and Anderson, F. C., 2006, "Using Computed Muscle Control to Generate Forward Dynamic Simulations of Human Walking From Experimental Data," J. Mech., **39**(6), pp. 1107–1115.

[16] Damsgaard, M., Rasmussen, J., Christensen, S. T., Surma, E., and de Zee, M., 2006, "Analysis of Musculoskeletal Systems in the AnyBody Modeling System," Simul. Model. Pract. Theory, **14**(8), pp. 1100–1111.

[17] Neptune, R. R., Clark, D. J., and Kautz, S. A., 2009, "Modular Control of Human Walking: A Simulation Study," J. Mech., **42**(9), pp. 1282–1287.

[18] Erdemir, A., McLean, S., Herzog, W., and van den Bogert, A. J., 2007, "Model-Based Estimation of Muscle Forces Exerted During Movements," Clin. Mech., **22**(2), pp. 131–154.

[19] Kim, J. H., Abdel-Malek, K., Xiang, Y., Yang, J., and Arora, J. S., 2011, "Concurrent Motion Planning and Reaction Load Distribution for Redundant Dynamic Systems Under External Holonomic Constraints," Int. J. Numer. Methods Eng., **88**(1), pp. 47–65.

[20] Piegl, L. A., and Tiller, W., 1995, *The NURBS Book*, Springer, Berlin.

[21] Prochazkova, J., 2005, "Derivative of B-Spline Function," 25th Conference on Geometry and Computer Graphics, Prague, Czech Republic.

[22] Holzbaur, K. R., Murray, W. M., and Delp, S. L., 2005, "A Model of the Upper Extremity for Simulating Musculoskeletal Surgery and Analyzing Neuromuscular Control," Ann. Biomed. Eng., **33**(6), pp. 829–840.

[23] Modenese, L., and Phillips, A. T. M., 2012, "Prediction of Hip Contact Forces and Muscle Activations During Walking at Different Speeds," Multibody Syst. Dyn., **28**(1–2), pp. 157–168.

[24] Gerritsen, K. G. M., van den Bogert, A. J., Hulliger, M., and Zernicke, R. F., 1998, "Intrinsic Muscle Properties Facilitate Locomotor Control—A Computer Simulation Study," Motor Control, **2**(3), pp. 206–220.

[25] Denavit, J., and Hartenberg, R. S., 1955, "A Kinematic Notation for Lower-Pair Mechanisms Based on Matrices," ASME J. Appl. Mech., **22**(2), pp. 215–221.

[26] Xiang, Y., Arora, J. S., and Abdel-Malek, K., 2009, "Optimization-Based Motion Prediction of Mechanical Systems: Sensitivity Analysis," Struct. Multidiscip. Optim., **37**(6), pp. 595–608.

[27] Sharifi, M., Salarieh, H., and Behzadipour, S., 2017, "Nonlinear Optimal Control of Planar Musculoskeletal Arm Model With Minimum Muscles Stress Criterion," ASME J. Comput. Nonlinear Dyn., **12**(1), p. 011014.

[28] Suzuki, M., Yamazaki, Y., Mizuno, N., and Matsunami, K., 1997, "Trajectory Formation of the Center-of-Mass of the Arm During Reaching Movement," Neuroscience, **76**(2), pp. 597–610.

[29] Ackermann, M., 2007, "Dynamics and Energetics of Walking With Prostheses," Ph.D. dissertation, University of Stuttgart, Stuttgart, Germany.

[30] Stansfield, B. W., Hillman, S. J., Hazlewood, M. E., and Robb, J. E., 2006, "Regression Analysis of Gait Parameters With Speed in Normal Children Walking at Self-Selected Speeds," Gait Posture, **23**(3), pp. 288–294.

[31] McLean, S. G., Su, A., and van den Bogert, A. J., 2003, "Development and Validation of a 3-D Model to Predict Knee Joint Loading During Dynamic Movement," ASME J. Biomech. Eng., **125**(6), pp. 864–874.

[32] Happee, R., 1994, "Inverse Dynamic Optimization Including Muscular Dynamics, a New Simulation Method Applied to Goal Directed Movements," J. Mech., **27**(7), pp. 953–960.

[33] Lemos, R. R., Epstein, M., Herzog, W., and Wyvill, B., 2004, "A Framework for Structured Modeling of Skeletal Muscle," Comput. Methods Biomech. Biomed. Eng., **7**(6), pp. 305–317.

[34] Farahani, S. D., Svinin, M., Andersen, M. S., de Zee, M., and Rasmussen, J., 2016, "Prediction of Closed-Chain Human Arm Dynamics in a Crank-Rotation Task," J. Mech., **49**(13), pp. 2684–2693.